

Analysis on mechanical behavior of dovetail mortise-tenon joints with looseness in traditional timber buildings

Yizhu Li^{1,2}, Shuangyin Cao^{*1,2} and Jianyang Xue³

¹Key Laboratory of Concrete and Prestressed Concrete Structures of Ministry of Education, Southeast University, Nanjing, P.R. China

²School of Civil Engineering, Southeast University, Nanjing, P.R. China

³School of Civil Engineering, Xi'an University of Architecture and Technology, Xi'an, P.R. China

(Received February 21, 2016, Revised October 3, 2016, Accepted October 6, 2016)

Abstract. To study the effect of looseness on mechanical behavior of dovetail mortise-tenon joints, five dovetail mortise-tenon joints, including one intact joint and four loose joints, were fabricated and tested under cycle lateral loadings, and non-linear finite element models using the software ABAQUS were also developed. The effects of looseness on stress distribution, rotational stiffness and bearing capacity of joints were studied based on the analysis of test and simulation results. The results indicate that the hysteretic loops are anti-Z-shaped and present typical characteristics of pinching and slippage, the envelop curves of joints are classified as following two stages: elastic and strengthening stage. The peak stress, rotational stiffness and bearing capacity of joints were reduced due to looseness. The moment-rotation theoretical model of intact joint was simplified in terms of the relation of construction dimensions for buildings, and the moment-rotation theoretical model considering the effect of looseness was proposed and validated.

Keywords: traditional timber building; dovetail mortise-tenon joint; looseness; finite element analysis; theoretical model

1. Introduction

Timber buildings have been used widely around the world in history, notably in China, Korea, Japan and Europe, for example, the *Blockhaus* structural system (timber log-walls) was a traditional construction technology and generally used in Italy and Portugal (Branco and Araujo 2012, Bedon, Fragiaco *et al.* 2015). In China, the timber buildings have been developed through long-term historic practices. The main architectural features for palace buildings in ancient China are mortise-tenon connection and bracket system, as shown in Fig. 1. The mortise-tenon connection is that the beam-end fabricated the shape of tenon is inserted into the column-end made the shape of mortise.

There are many types of mortise-tenon connection, which include dovetail mortise-tenon joint, penetrable mortise-tenon joint, semi-penetration mortise-tenon joint and so on. For the dovetail mortise-tenon joint, it is usually used to connect the architrave and column located in the external

*Corresponding author, Professor, E-mail: 101000873@seu.edu.cn



Fig. 1 Traditional timber building

aisle of palace buildings. According to the requirements of the *Engineering Fabrication Method of Chinese Qing Dynasty*, the dovetail mortise-tenon joint is composed of a pair of dovetail tenon and mortise with the inverted-trapezoid cross-section, there has been no clearance between the contact surfaces as the tenon is inserted into mortise.

In the past decades, the scholars have conducted a large amount of studies of ancient timber buildings. The researches on ancient timber frames have been extensively reviewed and summarized, which show that the connections of timber frames are semi-rigid (Leichti, Hyde *et al.* 2000, Chui and Li 2005, Villar, Guaita *et al.* 2007, D'Ayala and Tsai 2008, Santana and Mascia 2009, Zhang, Xue *et al.* 2011). For example, Villar, Guaita *et al.* (2007) conducted the finite element simulation of the timber frame. The result shows that the friction of contact surfaces is critical to the seismic performance of the structure, while the angle between members affects the stress distribution on the contact surfaces. D'Ayala and Tsai (2008) conducted the finite element analysis of the Dieh-Dou timber frame structure in Taiwan. The result indicates that the stiffness of joint has great influence on the displacement response of integral structure under earthquake, while the vertical load affects the rotational stiffness of the joint. Zhang, Xue *et al.* (2011) studied the dynamic characteristic and seismic response of palace structure model by shaking table test, which indicate that the reduction of seismic response of structure is mainly attributed to the friction-damping between the contact surfaces of connections and the friction-sliding between the plinth and cornerstone. Researchers also have studied kinds of timber joints and present varieties of connectional properties (Sandberg, Bulleit *et al.* 2000, Fang, Iwasaki *et al.* 2001, Li, Zhao *et al.* 2009, Parisi and Cordie 2010, Tannert, Lam *et al.* 2010, Chang, Thomson *et al.* 2011, Pang, Oh *et al.* 2011, Feio, Lourenco *et al.* 2014). For instance, Fang, Iwasaki *et al.* (2001) proposed the semi-rigid-link element that can reflect the mechanical characteristic of mortise-tenon joints to conduct the dynamic analysis of ancient timber architecture. Chang, Thomson *et al.* (2011) studied the rotational behavior of traditional Chuan-Dou timber joints in Taiwan, and the relationship of rotational stiffness and rotational angle was obtained.

Previous researches mainly focused on the dovetail mortise-tenon joint without looseness. In fact, some of the existing ancient timber buildings in China have been nearly a hundred or even

thousands of years. Most of the tenons were partially pulled out from the mortise due to the shrinkage, deformation and creep of timber, which caused the looseness of joint. The looseness has an important effect on the mechanical behavior of dovetail mortise-tenon joint. Therefore, based on the requirements of the *Engineering Fabrication Method of Chinese Qing Dynasty*, five 1:3.2 scaled dovetail mortise-tenon joints, including one intact joint and four loose joints, were fabricated and tested subjected to cyclic lateral loading. Efforts have been made to study the effect of looseness on the mechanical behavior of joints. In addition, the complex stress state of joints was analyzed by using the software ABAQUS. Besides, the theoretical model of moment-rotation considering looseness was proposed and validated.

2 Experimental program

2.1 Specimen design and fabrication

Five 1:3.2 scaled dovetail mortise-tenon joints were fabricated following requirements of the *Engineering Fabrication Method of Chinese Qing Dynasty*, including one intact joint and four loose joints, and the different degree of looseness of joints caused by the shrinkage and creep of timber was considered as analysis parameter. All the specimens have same dimensions. The sketch of specimen is shown in Fig. 2. Table 1 shows the dimensions of the members and dovetail mortise-tenon joints of both the prototype (studied example, Fig. 1) and the corresponding scaled specimens. The converse formula between the length unit of the Chinese Qing Dynasty and the international system of units is: 1 doukou=40 mm, where “doukou” is the basic length unit of the Chinese Qing Dynasty. The specimens were made of *pinus sylvestris* grown in the northeast areas of China, and the material properties tests of wood were carried out in terms of *Physical and mechanical tests of wood* (GB/1927-1943-91). The wood used for the specimens was not seasoned with kiln-drying. The moisture content of wood was 13.5%, and the density of wood was 0.48 g/cm^3 . The other material parameters of wood are reported in Table 2.

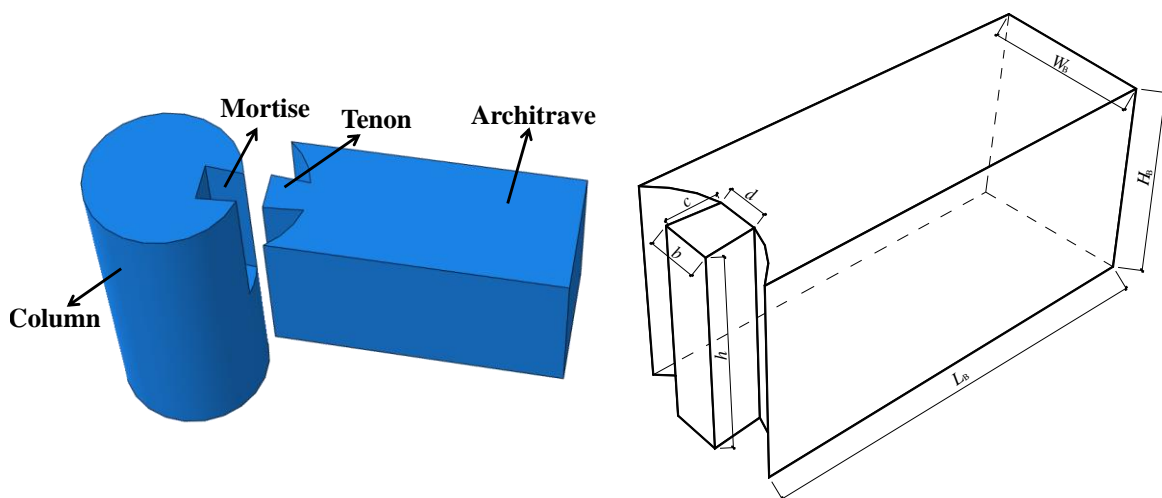


Fig. 2 Sketch of the dovetail mortise-tenon joints

Table 1 Prototype and model sizes

Member	L_C	D_C	L_B	H_B	W_B	h	b	d	c
Prototype (doukou)	25	6	20	6	4.8	6	1.5	1.2	1.5
Model (mm)	1000	240	800	240	190	240	60	50	60

Notes: “doukou” is the length unit of Chinese Qing Dynasty, L_C is the column length, D_C is the column diameter, L_B is the architrave length, H_B is the architrave height, W_B is the architrave width, h is the tenon height, b is the width of tenon forehead, d is the width of tenon neck, c is the tenon length.

Table 2 Mechanical properties of pinus sylvestris

ρ (g/cm ³)	ω (%)	E_L (MPa)	E_R (MPa)	E_T (MPa)	μ_{LR}	μ_{LT}
0.48	13.5	3805	268	154	0.5	0.1
μ_{RT}	G_{LR} (MPa)	G_{LT} (MPa)	G_{RT} (MPa)	f_L (MPa)	f_R (MPa)	f_T (MPa)
0.35	268	268	154	23.36	4.16	3.16

Notes: ρ is the density of wood, ω is the moisture content of wood, E_L is elastic modulus parallel to grain, E_R is elastic modulus perpendicular to grain along radial direction, E_T is elastic modulus perpendicular to grain along tangential direction, G_{RT} , G_{LR} , G_{LT} are shear modulus of cross section, radial section, tangential section respectively, μ_{RT} , μ_{LR} , μ_{LT} are Poisson's ratio of cross section, radial section, tangential section respectively, f_L is the compressive strength parallel to grain, f_R is compressive strength perpendicular to grain along radial direction, f_T is compressive strength perpendicular to grain along tangential direction.

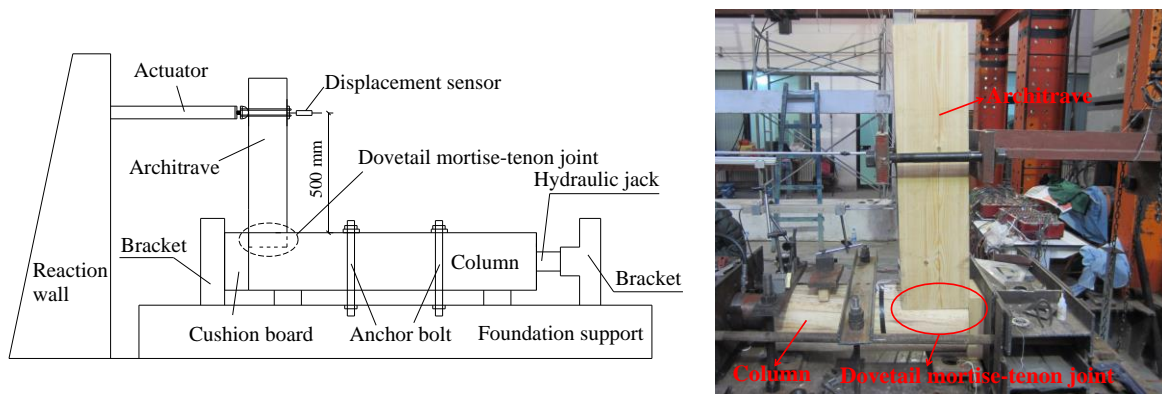


Fig. 3 Test setup

2.2 Test setup and loading program

The tests of specimens were carried out under cyclic lateral loading, and the test setup is shown in Fig. 3. Tests were performed in accordance with displacement-controlled. Loading reversals in push and pull direction were symmetric. When a given displacement was 5 mm, 10 mm, 15 mm, 20 mm and 25 mm, respectively, one loading cycle was applied for given displacement. Subsequently lateral loading were attempted three cycles for displacement of 30 mm, 35 mm, 40 mm, 45 mm, 50 mm and so on.

2.3 Definition of loose degree of joint

Table 3 Reduced sizes and loose degrees

Specimens	DJ1	DJ2	DJ3	DJ4	DJ5
Reductions of tenon length (mm)	0	5	8	12	16
Loose degrees D (%)	0	8.3%	13.3%	20.0%	26.7%

There are many factors causing the looseness of dovetail mortise-tenon joint, including shrinkage, deformation and creep of timber. Although the effects of these factors on looseness of joint were different extent, the final presentation modes of looseness of joint caused by these factors were similar, which presented that the tenon was partially pulled out from the mortise. Therefore, the method of reducing tenon length was used to simulate looseness of dovetail mortise-tenon joints, which caused by the shrinkage, deformation and creep of timber. The greater the loose degree of joint is, the greater the reduction of tenon length is. For the convenience of analyzing the influence of looseness on the mechanical behavior of joints, the loose degree (D) was defined as the ratio of the reduction of tenon length to the original length of tenon. The specific details of joints are listed in Table 3.

3 Finite element simulation

If purely based on experimental work, it would be almost impossible to obtain stress distributions within a joint. Therefore, it is necessary to develop a numerical model to simulate the joints by using nonlinear finite element analysis. With finite element models validated by the related experimental results, stress and strain distributions in any critical areas of the joints can be investigated. In this phase of the study, nonlinear finite element models of the joints were developed using the software ABAQUS.

3.1 Constitutive relationships and material properties

Both the column and architrave were modeled as orthotropic materials, elastic-perfectly plastic model and elastic-perfectly model were undertaken in compression and tension along the grain of wood respectively, and the elastic modulus of tension parallel to grain is equal to that of compression parallel to grain, the stress-strain relationship of timber parallel to grain is shown in Fig. 4. The elastic-plastic model considering strain hardening and elastic-perfectly model were utilized for compression and tension perpendicular to grain of wood respectively, and the elastic modulus of tension perpendicular to grain is equal to that of compression perpendicular to grain. Based on the material test results, the hardening stiffness of $E_{R,tan}$ and $E_{T,tan}$ were 0.3 times the elastic stiffness of E_R and E_T respectively after the wood passed into the plasticity in the direction of cross grain, and the stress-strain relationship of timber perpendicular to grain is shown in Fig.5. The details of material parameters are shown in Table 2. In ABAQUS software, material orthotropic was defined using the "Engineering Constants" in the elastic stage of wood, and the "potential" function of ABAQUS/Standard was applied to define the different yield stresses in all directions of timber. A Hill yield criterion for compression and a Rankine yield criterion for tension were adopted.

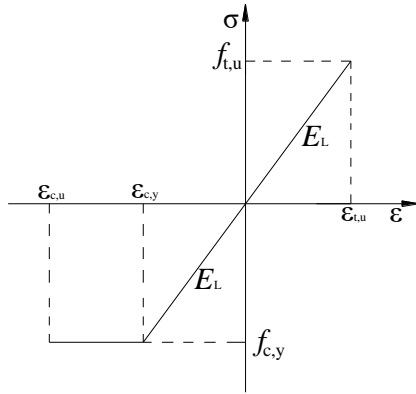


Fig. 4 Stress-strain relationship of timber parallel to grain

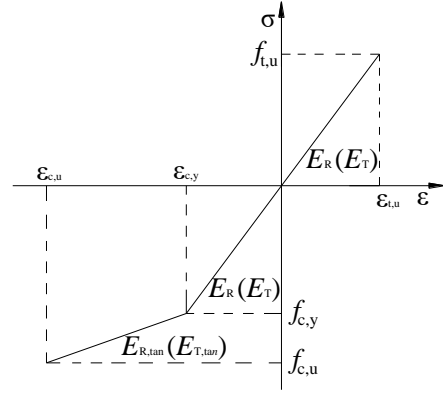


Fig. 5 Stress-strain relationship of timber perpendicular to grain

3.2 Modeling of interactions

The interactions of contact surface between the tenon and mortise were simulated by the “General Contact” of ABAQUS/Standard, the contact properties of interfaces were divided into normal and tangential behaviors. The “hard contact” of ABAQUS/Standard was used to simulate the normal behavior, and the contact surfaces were allowed to separation in the loading progress. The interaction, tangential to the contact surface, is termed as shear stress, which was used to simulate the friction force of the contact surface between the tenon and mortise. The magnitude of sliding that occurs, however, is governed by the limiting resistive friction force given as follow

$$f = \mu p \tag{1}$$

where f is limiting friction force, p is contact pressure acting normal to the contact surface and μ is coefficient of friction, which ranged from 0.26 to 0.34 based on the previous results by Chen *et al.* (2010), and 0.3 was taken in this paper.

In ABAQUS/Standard, the contact problem was defined by pairing of the surfaces that were likely to come into contact during simulation and by specifying the type of interaction they would experience. To simulate contact it was necessary to identify the areas within a contact pair actually in contact or out of contact, then to apply and remove constraints over these surface areas, and finally to calculate the magnitude of contact pressures and shear stresses.

3.3 Mesh generation and boundary conditions

In this work, each member (Column, Architrave) was modeled, as an architrave having a regular $0.021 \times 0.021 \text{ m}^2$ -cross section and consisting of three-dimensional elements, but the column having an irregular approximate size 0.017 m due to irregularity of column. Based on preliminary sensitivity studies, an extremely fine mesh of eight-node linear brick (C3D8R) 3D-stress solid elements was used. The eight-node elements allowed the user to correctly describe the nominal geometry of members, both along their main body and dovetail mortise-tenon joints and to ensure accuracy of interaction formulations. To ensure that the column could not motion in the process of loading, the two reference points (RP-1, RP-2) coupled with the ends of the column

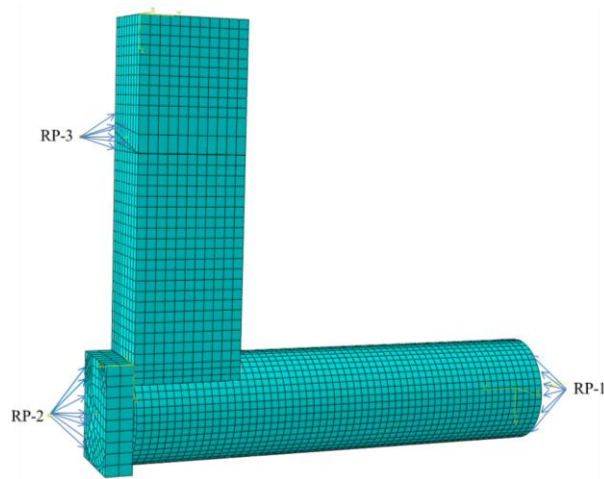


Fig. 6 Mesh generation and boundary conditions

respectively for the convenience of applying boundary conditions were restrained ($u_x=u_y=u_z=0$). Similarly, a reference point (RP-3) was set to couple the horizontal displacement loading surface. The horizontal in-plane lateral displacement was applied to the reference point (RP-3) as quasi-static, linearly increasing time-varying displacement, which was similar to the loading program. The mesh generation and boundary conditions were shown in Fig. 6.

4 Results and discussion

4.1 Failure modes

Fig. 7 shows the failure modes of joints. The main failure modes of all joints were consistent, thus the failure modes of DJ1 were elaborated as an example. In the early stages of loading, tenon and mortise squeezed each other on the contact surfaces and the specimens squeaked, which contributed for elastic compressive deformation on the contact surface. With the increase of lateral loading displacement, the plastic compressive deformation was observed on the interface areas and the wood fiber was cocked at the vicinity of mortise. When the rotational angle of joint reached about 0.08 rad, the architrave was uplifted due to the enlarged mortise induced by squeezing, and then dropped down all of a sudden owing to the gravitational effects as architrave returned to equilibrium position of loading. Finally, the tenon was partially pulled out and the specimen failed since the lateral loading displacement was excessively large. For the dovetail mortise-tenon joints with different loose degrees, the compressive deformation located on the contact surface decreased with the increase of loose degree, and the wood fiber was cocked slightly at the vicinity of mortise, while the pulling-out rates of tenon (the ratio of pulling-out length of tenon to the tenon length) increased.

4.2 $M-\theta$ hysteretic loops of joints

In this paper, the $M-\theta$ relationship could be obtained in terms of the $P-\Delta$ relationship, the

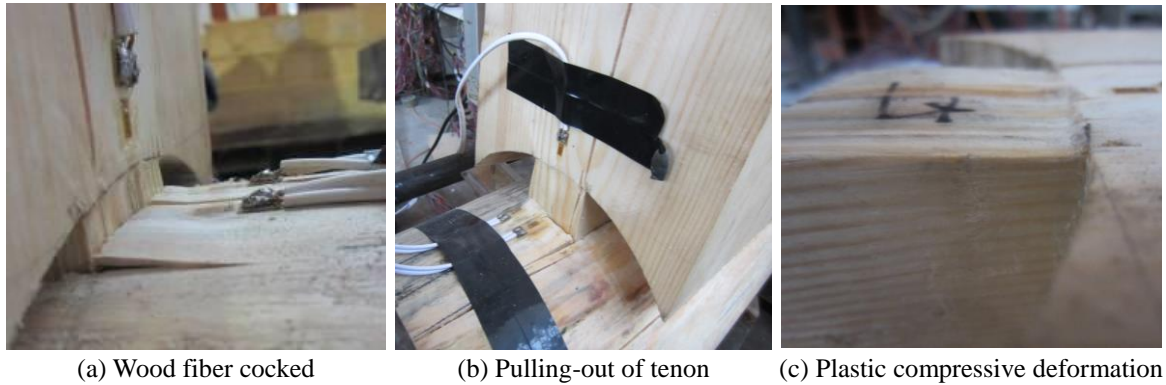


Fig. 7 Failure modes

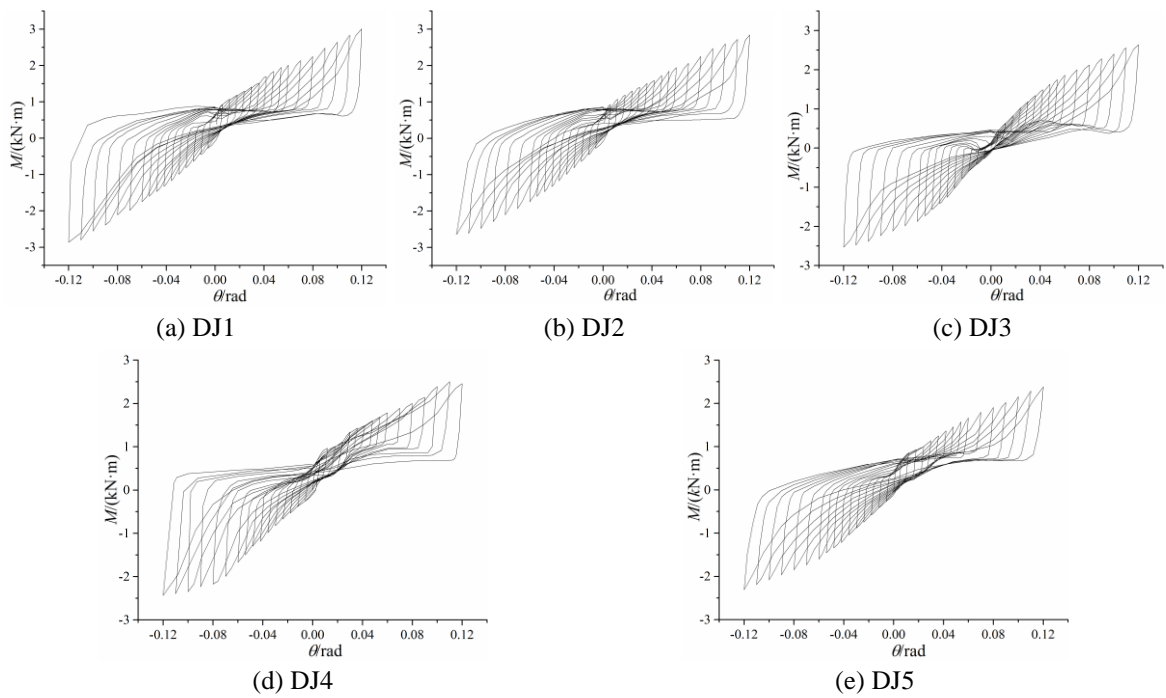
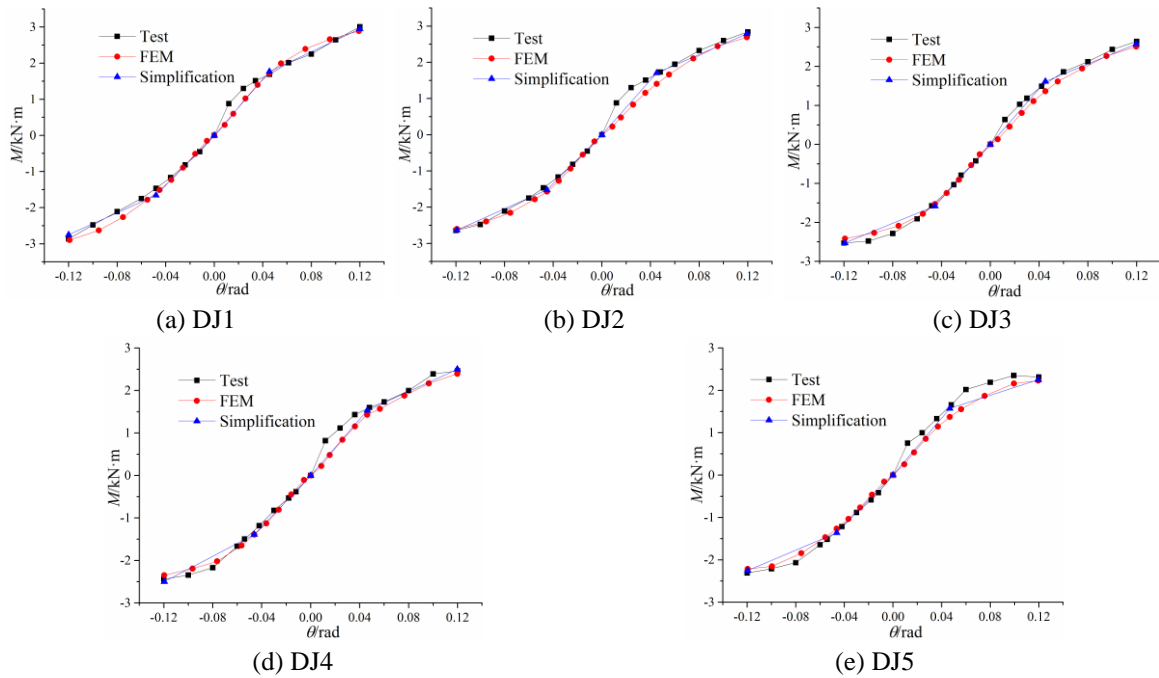


Fig. 8 Moment-rotation hysteretic loops

bending moment (M) was defined as an applied load (P) multiplied by the distance from the loading point to the centre of rotation in the architrave, and the rotational angle (θ) was defined as the ratio of the horizontal displacement (Δ) in the loading point to the distance described above. The M - θ hysteretic loops of joints were shown in Fig. 8. All five scaled specimens developed stable responses up to the cyclic amplitude of 0.12 rad. An S-shaped hysteretic loop was initiated in the early stages of loading. The specimens developed an anti-Z-shaped hysteretic loop with the increasing loading displacement, and the pinching and slippage effect on the hysteretic loop can be found for any relatively larger displacement, which indicated the degradation of the energy dissipation and a great deal of slippage on the contact surface between the tenon and mortise.

Fig. 9 Comparison of M - θ envelope curves

When the specimen was unloaded at a large displacement, the unloading curve was almost perpendicular to the horizontal axis, which means the displacement decreased slightly with the restoring force decreasing to zero and a large residual displacement was left, which was consistent with previous research results by Chun, Yue *et al.* (2011), Li, Zhao *et al.* (2015). With the increase of loose degree of joints, the pinching effect of hysteretic loops increased and the area of hysteretic loops was reduced under the same displacement load level, which suggest that the friction-sliding effect of joints increased and the energy dissipation capacity decreased.

4.3 M - θ envelope curves of joints and model validation

The M - θ envelope curves could be divided into the following two stages according to its mechanical characteristics: elastic and strengthening stage, as shown in Fig. 9. When the lateral loading displacement was small, the curve slope was relatively large and the elastic deformation was generated on the contact surface between tenon and mortise in the elastic stage. As the rotational angle increased about 0.04 rad, the curve gradually inclined to the horizontal axis and the plastic compressive deformation was observed on the interface areas. Meanwhile, the joint passed into the strengthening phase, which was consistent with previous studies by Chun, Yue *et al.* (2011), Li, Zhao *et al.* (2015). Comparing the M - θ envelope curves of joints with different loose degree, the envelope curves were substantially similar for the joints in the elastic stage. The bending moment of joints was reduced slightly with the increase of loose degree, and the maximum reduction was 7.8%. When the rotational angle of joints exceeded 0.04rad, the reduction of bending moment of joints increased obviously with the increase of loose degree, and the maximum reduction of bending moment was 21% as the rotational angle of joints reached 0.12

rad. Fig. 9 also shows the comparison of simulation and test curves, and reasonably good correlation could be seen in the diagram, which showed that the established finite element model satisfied certain credibility. At the beginning of loading, the deviations of simulated and experimental results were relatively large, which could be attributed to the following two reasons: one was that the friction coefficient defined on the contact surfaces of model was smaller than that in test, thus the initial rotational stiffness obtained from the test was larger than that obtained from the simulation. The other was that the tenon and mortise squeezed each other in the early loading since the architrave and column were difficult to maintain in the identical plane, which led to the increased rotational stiffness of joints.

4.4 Stress distribution analysis

4.4.1 Stress distribution analysis of tenon

The stress distribution of tenon was shown in Fig. 10 as the rotational angle of joint reached ultimate rotation. Since one side of the tenon was partially pulled out from the mortise, the compressive stress could be observed on the contact surfaces between the side surface of tenon and mortise. The compressive stress on the contact surface could be decomposed into tensile stress parallel to grain S11 and compressive stress perpendicular to grain along the tangential direction S33. For tensile stress along the grain direction S11, the tensile stress was small and mainly appeared in architrave root in the early stage of loading. While the tensile stress began to shift along the longitudinal direction of tenon owing to the pulling-out of tenon with the increase of loading displacement. When the rotational angle of joint achieved ultimate rotation, the maximum stress of 14.29 MPa located on the upper of the contact surface was less than the tensile strength along the grain of 23.36 MPa. Meanwhile, the stress could be observed in the middle section of the architrave root and decreased gradually to both sides in a triangular shape. The compressive stress perpendicular to grain along the radial direction S22 was generated on the upper surface of tenon due to the rotation of the tenon. In the early of loading, the maximum compressive stress could be observed on the neck region of tenon. Then, the stress was transferred to the forehead of tenon due to the pulling-out of tenon with the increasing loading displacement. The maximum compressive stress began to over the compressive strength perpendicular to grain along the radial direction, and the shape of stress area was trapezoid. When the rotational angle of joint reached ultimate rotation,

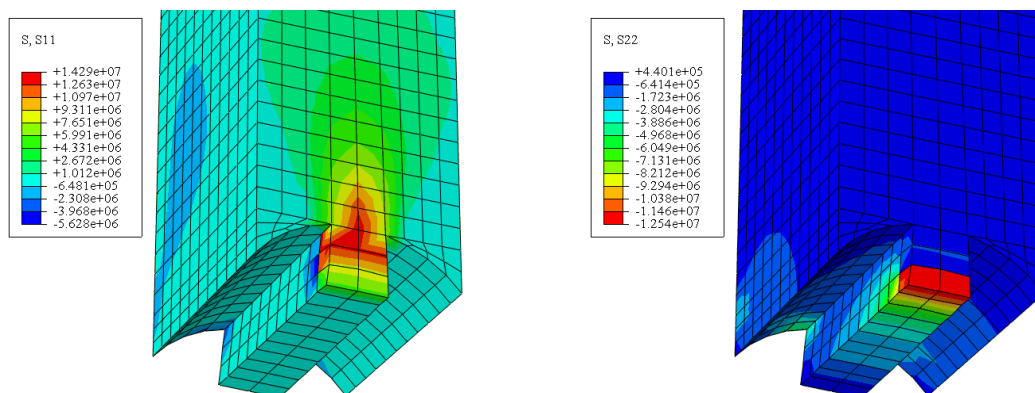


Fig. 10 Tenon stress corresponding to ultimate rotation (units: Pa)

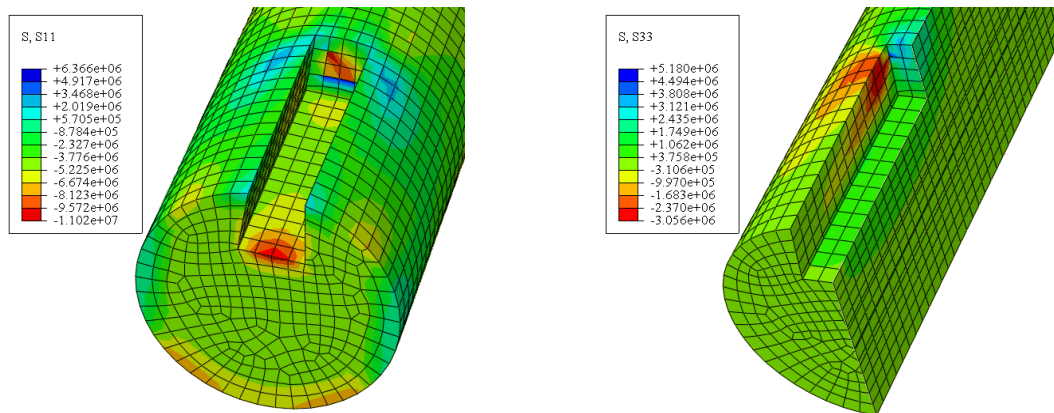


Fig. 11 Mortise stress corresponding to ultimate rotation (units: Pa)

the maximum stress of 12.54 MPa appeared on the forehead of tenon was far larger than the compressive strength perpendicular to grain along the radial direction of 4.16 MPa. Therefore, the wood was in second stage of strain hardening.

4.4.2 Stress distribution analysis of mortise

Fig. 11 shows the stress distribution of mortise as the rotational angle of joint reached ultimate rotation. The tensile stress perpendicular to the side surface of mortise was generated due to the pulling-out of one side of tenon. And the tensile stress could be decomposed into tensile stress perpendicular to grain along the radial direction S22 and compressive stress perpendicular to grain along the tangential direction S33. For compressive stress along the tangential direction S33, the stress was located on the bottom of side surface of mortise in the early stage of loading, and the shape of stress area was triangle. With the increasing pulling-out length of tenon, the stress was transferred to the upper of side surface of mortise and the triangle region of stress decreased gradually. When rotational angle of joint reached ultimate rotation, the maximum stress of 3.06 MPa was less than the compressive strength perpendicular to grain along the tangential direction. Since the upper surface of tenon and the bottom surface of mortise squeezed each other, the compressive stress S11 was produced on the bottom surface of mortise. At the beginning of loading, the stress was observed on the bottom of contact surface and presented in trapezoidal shape. While the stress began to extend toward the upper of the contact surface with the pulling-out of tenon and the trapezoidal area of stress increased. The maximum stress was 11.02 MPa as the rotational angle of joint reached ultimate rotation, which was less than the compressive strength parallel to grain of 23.36 MPa.

4.5 Impact analysis of looseness

4.5.1 Stress state distribution

According to numerical analysis for dovetail mortise-tenon joints with different loose degrees, the maximum stress shown in Table 4 could be obtained when rotational angle of joint reached ultimate rotation. For the tensile stress parallel to grain of tenon S11, the maximum stress was located on the upper surface adjoined the neck of tenon and decreased significantly with the increase of loose degree. For the stress perpendicular to grain of tenon S22 and S33, the maximum

Table 4 Stress of tenon and mortise

Specimens	Loose degree D (%)	Tenon stress (MPa)			Mortise stress (MPa)		
		S11	S22	S33	S11	S22	S33
DJ1	0	14.3	-12.5	-8.1	-8.5	3.1	5.2
DJ2	8.3	11.1	-10.9	-7.9	-6.2	2.9	5.0
DJ3	13.3	10.1	-8.2	-6.4	-5.1	2.7	4.9
DJ4	20.0	8.1	-7.2	-5.9	-6.5	2.8	4.8
DJ5	26.7	7.2	-7.0	-5.5	-6.1	2.8	4.4

Notes: S11 is the stress parallel to grain of timber, S22 is the stress perpendicular to grain along radial direction of timber, S33 is the stress perpendicular to grain along tangential direction of timber.

Table 5 Stiffness of joints

Specimens	Loose degrees D (%)	Elastic stiffness K_1 (kN·m/rad)		Strengthening stiffness K_2 (kN·m/rad)	
		Test	Simulation	test	Simulation
DJ1	0	36.74	37.33	16.94	15.82
DJ2	8.3	35.05	31.18	14.89	15.08
DJ3	13.3	32.81	30.27	12.99	13.80
DJ4	20.0	30.13	30.09	12.20	13.11
DJ5	26.7	28.80	29.42	9.63	10.61

stress was observed on the upper surface adjoined the forehead of tenon and similarly increased with the increase of loose degree of joints. This is because the distance from the rotational point to the forehead of tenon decreased due to the decreasing tenon length, which induced relatively smaller compressive stress on the contact surface between the tenon and mortise.

For the compressive stress along the grain of mortise S11, the maximum stress was located in the middle section of the bottom surface of mortise and the shape of the stress region was trapezoidal. With the increase of loose degree of joints, the maximum stress shifted to the upper of the bottom surface of mortise and the area of stress was reduced, while the ultimate stress decreased first and then increased. For the stress perpendicular to grain of mortise S22 and S33, the maximum stress was found on the lower and upper of side surface of mortise respectively, and the shape of stress region was triangle. As the loose degree of joints increased, the maximum stress was reduced slightly and the area of stress region was basically constant. This is because the stress perpendicular to grain of mortise could not dominate the behavior of joints.

4.5.2 Rotational stiffness

Through the above-mentioned analysis of envelope curves of joints, the envelope curves could be divided into the following two stages according to its mechanical characteristics: elastic and strengthening stage, where K_1 denoted the elastic stiffness of joints, K_2 denoted the strengthening stiffness of joints. And the specific stiffness of joints was shown in Table 5.

Compared with the elastic stiffness of DJ1, the elastic stiffness of DJ2, DJ3, DJ4 and DJ5 were 4.6%, 10.7%, 18.0 % and 21.6% lower, respectively. It indicates that the elastic stiffness of joints decreased with the increase of loose degree of joints. This is because the rotational stiffness of joint was related to the compressive stress located on the contact surface between the tenon and

Table 6 Bearing capacity and the corresponding degradation rate of joints

Specimens	Loose degrees D (%)	Bearing capacity M_u (kN·m)		Degeneration rate of bearing capacity λ (%)
		Test	Simulation	
DJ1	0	3.01	2.89	0
DJ2	8.3	2.84	2.69	5.6
DJ3	13.3	2.64	2.51	12.3
DJ4	20.0	2.46	2.39	18.3
DJ5	26.7	2.32	2.23	22.9

mortise, while the compressive stress was reduced with the increase of the loose degrees of joints as stated in stress analysis. After the joints passed into the strengthening stage, the contact surface generated plastic compressive deformation and the strengthening stiffness of joints were significantly lower than the elastic stiffness. Comparison of the strengthening stiffness of joints, the strengthening stiffness of joints decreased similarly with the increase of loose degree of joints. Compared to DJ1, the strengthening stiffness of DJ2, DJ3, DJ4 and DJ5 were lower by 12.1%, 23.3%, 30.0% and 43.2%, respectively. Comparison the reductions of elastic stiffness and strengthening stiffness of joints, the reductions of strengthening stiffness were greater than those of elastic stiffness significantly.

4.5.3 Bearing capacity

Table 6 shows the influence of looseness on bearing capacity and the corresponding degradation rate of joints. The degradation rate of bearing capacity of loose joints was defined as the ratio of bearing capacity reduction of loose joint to bearing capacity of intact joint. As shown in Table 6, the bearing capacity of joints decreased while the degradation rate of bearing capacity of joints increased with the increase of loose degree. The relationship of the degradation rate of bearing capacity λ and the loose degree of joint D determined through the regressive analysis was expressed as

$$\lambda = -7.49 + 179.66D - 247.65D^2 \quad (2)$$

The bearing capacity was relevant to the contact area and compressive stress generated on the contact surface between the tenon and mortise. The compressive stress, as stated in the stress analysis, was decreased with the increase of loose degree. And the greater the loose degree of joints was, the smaller the contact area was. Therefore, the bearing capacity was reduced with the increase of loose degree of joints.

4.6 Theoretical model of M - θ and validation

4.6.1 Theoretical model simplification and validation

The M - θ theoretical model of dovetail mortise-tenon joint was proposed by Xie, Du *et al.* (2014). The calculation formulas were given as follows:

$$M = \frac{IE_R(\theta) \sin \theta \cos \theta}{2h} (dl_{c,b}^2 - bl_{c,t}^2 \cos \theta) - \frac{\mu l h^2 E_R(\alpha)(b-d)(2c-h\theta)\theta \cos^3 \theta}{2c(b+d) \cos \alpha} \quad (3)$$

$$l_{c,t} = \frac{d \cos [h - L \sin (\theta + \varphi)]}{\mu b - d \sin \theta \cos ^2 \theta} + \sqrt{\frac{h \theta (b - d) E_R(\alpha) E_R(\theta) (2c - h \theta)}{2c(b + d) \cos \alpha} (\sin \alpha + \mu \sin \theta) \sin \theta [\mu b - d \sin \theta (\cos \theta)^2]} + \sqrt{\frac{\mu b d E_R^2(\theta) \sin \theta \left[\frac{2l}{h} \sin (\theta + \varphi) - 1 - \frac{L^2}{h^2} \sin^2 (\theta + \varphi) \right]}{\frac{\mu b}{h} E_R(\theta) \sin \theta - \frac{d}{h} E_R(\theta) \sin^2 \theta \cos^2 \theta}} \quad (4)$$

$$l_{c,b} = \frac{L \sin (\theta + \varphi) - h - l_{c,t} \sin \theta \cos \theta}{\tan \theta} \quad (5)$$

$$E_R(\theta) = E_R \chi(\theta), \varepsilon < \varepsilon_y \quad (6)$$

$$E_{R,tan}(\theta) = E_{R,tan} \chi(\theta), \varepsilon_y < \varepsilon < \varepsilon_u$$

$$\chi(\theta) = \frac{E_L}{E_L \cos^n \theta + E_R \sin^n \theta} \quad (7)$$

$$L = \sqrt{h^2 + c^2} \quad (8)$$

$$\varphi = \arctan \frac{h}{c} \quad (9)$$

where M is bending moment of joint, θ is the rotational angle of joint, l is the distance from the loading point to the rotation point of tenon, μ is friction coefficient of contact surface between the tenon and mortise, h is the tenon height of joint, c is tenon length of joint, b is width of tenon forehead, d is width of tenon neck, α is narrow angle of tenon, $l_{c,b}$ 、 $l_{c,t}$ shown in Fig. 12 are the length of embedded regions of tenon respectively, $\chi(\theta)$ is amplifying coefficients of elasticity modulus corresponding to the slope of θ for timber, n is intensity impact factor caused by wood species, $E_R(\theta)$ is the elasticity modulus perpendicular to grain at the slope of θ for timber, $E_{R,tan}(\theta)$

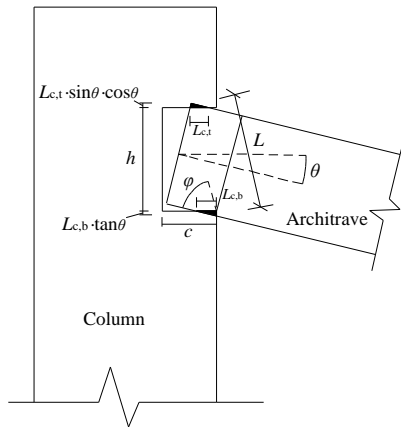


Fig. 12 Dimensions of dovetail mortise-tenon joint

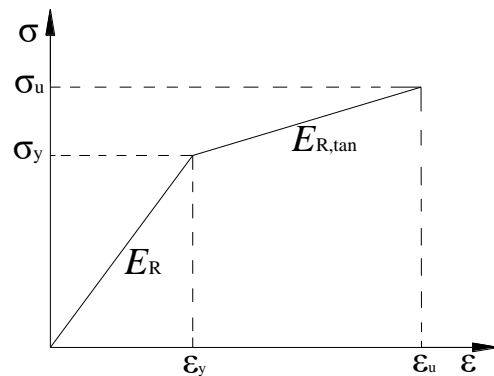


Fig. 13 Stress-strain relationship of cross grain at the radial direction

is the modulus perpendicular to grain at the slope of θ for timber passed into strain hardening and the constitutive relationship of compression perpendicular to grain was shown in Fig. 13.

The formulas of $l_{c,b}$ and $l_{c,t}$ were extremely complex and not convenient for practical application. Thus, the formulas of theoretical model could be simplified in terms of the relation of construction dimensions for buildings fabricated following requirements of the *Engineering Fabrication Method of Chinese Qing Dynasty*. The following simplification can be made:

(1) For the buildings made following requirements of the *Engineering Fabrication Method of Chinese Qing Dynasty*, the relationship of dimension parameters could be expressed as the column diameter R is equal to the tenon height h , the tenon length c is 0.25 to 0.3 times the column diameter R , the width of tenon forehead b is equal to the tenon length c , the width of tenon neck d is 0.83 times the width of tenon forehead b and the narrow angle of tenon α is 0.083rad.

(2) Since the narrow angle of tenon α and the rotational angle of joints θ were small, the parameters of $\sin\alpha$, $\cos\alpha$, $\sin\theta$, $\tan\theta$, $\cos\theta$, $\cos^2\theta$ and $\cos^3\theta$ could be approximately given 1. By the $\varphi=1.33$ rad, the parameter of $\sin(\theta+\varphi)$ could also be approximately taken 1.

(3) The compressive elastic modulus parallel to grain E_L is 10 to 20 times the compressive elastic modulus perpendicular to grain E_R for wood (Chinese standard 2005), the intensity impact factor (n) could be given 3.1 (Ma *et al.* 2012), and the angle of θ and α are small. Therefore, the parameters of $\chi(\theta)$, $\chi(\alpha)$, $E_R(\theta)$, $E_R(\alpha)$, $E_{R,tan}(\theta)$ and $E_{R,tan}(\alpha)$ could be expressed as

$$\chi(\theta) = \chi(\alpha) = 1 \quad (10)$$

$$E_R(\theta) = E_R(\alpha) = E_R, \varepsilon < \varepsilon_y \quad (11)$$

$$E_{R,tan}(\theta) = E_{R,tan}(\alpha) = E_{R,tan}, \varepsilon_y < \varepsilon < \varepsilon_u$$

The simplified theory model of $M-\theta$ was developed in light of the above simplification of parameters, and the formulas of simplified theory model could be expressed as follows

$$M = \frac{IE_R\theta[(55l_b^2 - 66l_t^2) - \mu h^2(48 - 96\theta)]}{528} \quad (12)$$

$$l_{c,t} = \frac{5 \cos[\frac{4 - \sqrt{17}}{4}h]}{6\mu - 5\theta} + \frac{h\sqrt{(1 - 2\theta)(0.083 + \mu\theta)(6\mu - 5\theta)\theta^2 - 0.013\theta}}{0.677\theta(6\mu - 5\theta)} \quad (13)$$

$$l_{c,b} = \frac{(\sqrt{17} - 4)h}{4\theta} - l_{c,t} \quad (14)$$

To validate the reasonability of simplified theory model, Fig. 14 shows the comparison of the calculation results and the test results obtained for intact joint of DJ1 based on the parameters of joint shown in Table 7. It could be seen in the Fig. 14 that the calculation results were well in agreement with the experimental results, which indicated that the simplified theory model had certain credibility and the simplified parameters could ensure reasonable results.

4.6.2 Theoretical model considering influence of looseness

According to the analysis of the results of test and simulation, the mechanical behavior of dovetail mortise-tenon joints decreased obviously after the looseness of joint. Therefore, it was

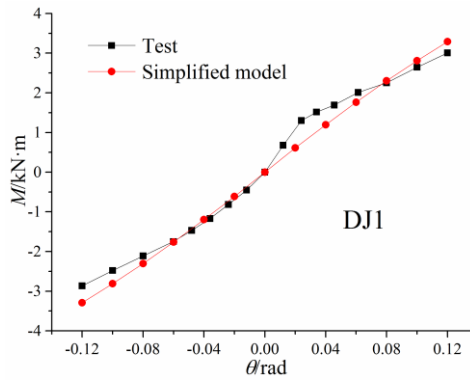


Fig. 14 Comparison of results

Table 7 Parameters of joint

h (mm)	c (mm)	d (mm)	b (mm)	L (mm)	E_R (MPa)	$E_{R,tan}$ (MPa)	μ	α (rad)	l (mm)
240	60	50	60	247.4	268	81	0.3	0.083	500

Table 8 Bending moments of joints

Specimens	θ (rad)	M (kN·m)					
		0.02	0.04	0.06	0.08	0.100	0.12
DJ1		1.08	1.62	2.01	2.30	2.65	3.01
DJ2		0.97	1.58	1.94	2.16	2.35	2.84
DJ3		0.86	1.46	1.86	2.17	2.24	2.64
DJ4		0.80	1.42	1.73	2.04	2.19	2.46
DJ5		0.84	1.38	1.82	1.96	2.07	2.32

necessary to establish the M - θ theoretical model of dovetail mortise-tenon joints considering the influence of looseness. In the above-mentioned analysis, the bending moments of loose joints were lower than those of intact joint at different rotational angle of joints, and the bending moments of joints were shown in Table 8. The theoretical model of joints considering looseness could be established through nonlinear regression analysis, the M - θ relationship of loose joints and intact joint were given as

$$\frac{M(\theta, D)}{M(\theta)} = 0.81 - 1.34D + 6.76\theta + 2.90D^2 - 44.40\theta^2 + 0.32D\theta \tag{15}$$

where $M(\theta)$ is the bending moment of intact joint at the rotational angle of θ , $M(\theta, D)$ is the bending moment of joint with the loose degree of D at the rotational angle of θ , θ is the rotational angle of dovetail mortise-tenon joint, D is the loose degree of dovetail mortise-tenon joint.

To validate the reasonability of theoretical model considering influence of looseness, Fig. 15 shows the comparison of theoretical calculation results and experimental results of joints with different loose degrees. It was noticed that the reasonable correlation was obtained, which illustrated that the theoretical model considering the influence of looseness could well reflect the mechanical behavior of dovetail mortise-tenon joints with different loose degrees.

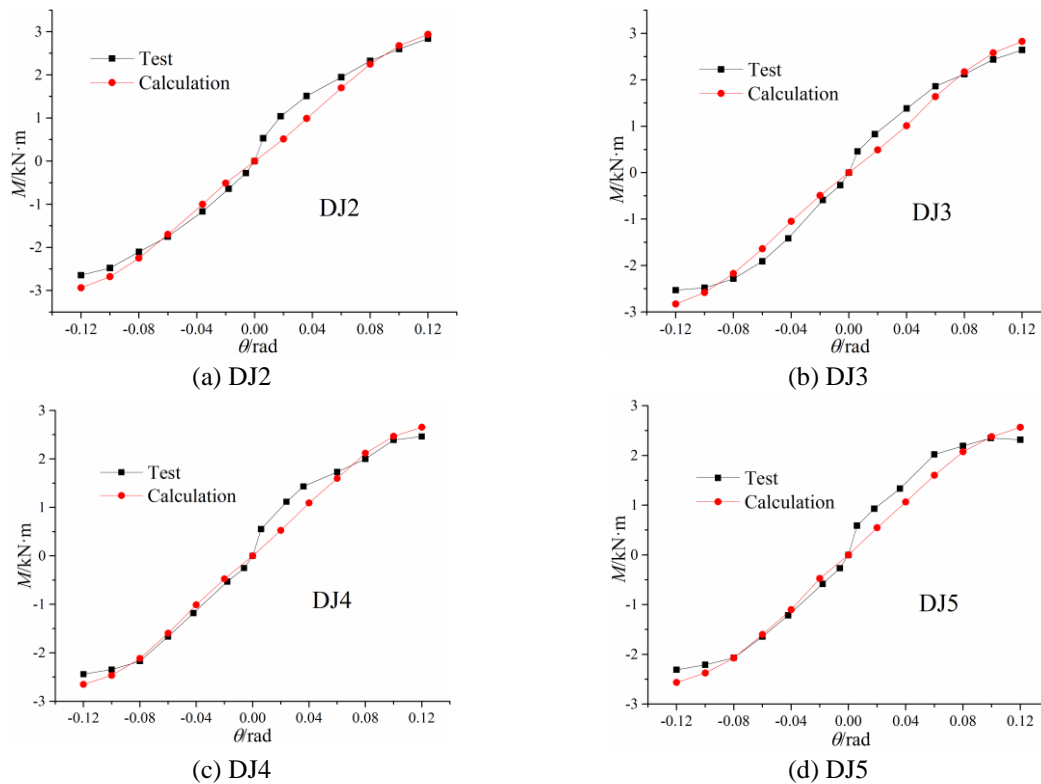


Fig. 15 Comparison of calculation results and test results

5. Conclusions

Five dovetail mortise-tenon joints with different loose degrees have been experimentally and numerically studied. Based on the analyses on test results and comparisons with the results of finite element model, the following conclusions could be pointed out:

- The final failure modes of dovetail mortise-tenon joints were that the tenon was partially pulled out and the severe extrusion deformation appeared on the contact between the tenon and mortise. The hysteretic loops of joints were anti-Z-shaped and the envelope curves of joints were divided into the following two stages according to its mechanical characteristics: elastic and strengthening stage. The mechanical behavior of joints was degraded with the increase of the loose degree of joints.
- Through the establishment of finite element model of dovetail mortise-tenon joints, the stress distribution of tenon and mortise in critical areas were studied in detail. The stress perpendicular to grain on the contact surface between the tenon and mortise could exceed the critical stress of timber.
- The looseness had an obvious effect on the stress distribution, rotational stiffness and carrying capacity of dovetail mortise-tenon joints.
- The M - θ theoretical model considering influence of looseness has been proposed based on the simplification of M - θ theoretical model, and the analytical results were well in agreement with the experimental results.

Acknowledgements

The work presented herein was carried out at Southeast Univ. in China, and was funded by Chinese State “twelfth five-year” Science and Technology Support Plan under granted No. 2012BAJ14B02. Chinese National Natural Science Foundation under granted No.51678478. The financial support provided by the funding agency is gratefully acknowledged.

References

- Bedon, C. and Fragiacomio, M. (2015), “Numerical and analytical assessment of the buckling behaviour of *Blockhaus* log-walls under in-plane compression”, *Eng. Struct.*, **82**, 134-150.
- Bedon, C., Fragiacomio, M. and Amadio, C. (2015), “Experimental study and numerical investigation of *blockhaus* shear walls subjected to in-plane seismic loads”, *J. Struct. Eng.*, **141**(4), 1-11.
- Bedon, C., Rinaldin, G. and Izzi, M. (2015), “Assessment of the structural stability of *Blockhaus* timber log-walls under in-plane compression via full-scale buckling experiments”, *Constr. Build. Mater.*, **78**, 474-490.
- Branco, J.M. and Araujo, J.P. (2012), “Structural behaviour of log timber walls under lateral in-plane loads”, *Eng. Struct.*, **40**, 371-382.
- Chang, W.S., Thomson, A. and Harris, R. (2011), “Development of all-wood connections with plywood flitch plate and oak pegs”, *Adv. Struct. Eng.*, **14**(2), 123-132.
- Chen, Z.Y. (2010), “Behavior of typical joint and the structure of YingXian wood pagoda”, Ph.D. Dissertation, Harbin University of Technology, Harbin, China.
- Chinese standard (2005), *Timberwork design manual*, China Architecture & Building Press, Beijing, China.
- Chui, Y.H. and Li, Y.T. (2005), “Modeling timber moment connection under reversed cyclic loading”, *J. Struct. Eng.*, **131**(11), 1757-1763.
- Chun, Q., Yue, Z. and Pan, J.W. (2011), “Experimental study on seismic characteristics of typical mortise-tenon joints of Chinese southern traditional timber frame buildings”, *Sci. China: Technol. Sci.*, **54**(9), 2404-2411.
- D’Ayala, D.F. and Tsai, P.H. (2008), “Seismic vulnerability of historic Dieh-Dou timber structures in Taiwan”, *Eng. Struct.*, **30**, 2101-2113.
- Fang, D.P., Iwasaki, S. and Yu, M.H. (2001), “Ancient Chinese timber architecture. I: experimental study”, *J. Struct. Eng.*, **127**(11), 1348-1357.
- Fang, D.P., Iwasaki, S. and Yu, M.H. (2001), “Ancient Chinese timber architecture. II: dynamic characteristics”, *J. Struct. Eng.*, **127**(11), 1358-1364.
- Feio, A.O., Lourenco, P.B. and Machado, J.S. (2014), “Testing and modeling of a traditional timber mortise and tenon joint”, *Mater. Struct.*, **47**(1), 213-225.
- GB/1927-1943-91 (1991), *Physical and mechanical tests of wood*, China technical committee for standardization of timber, Beijing, China.
- Leichti, R.J., Hyde, R.A. and French M.L. (2000), “The continuum of connection rigidity in timber structures”, *Wood Fiber Sci.*, **32**(1), 11-19.
- Li, X.W., Zhao, J.H. and Ma, G.W. (2015), “Experimental study on the seismic performance of a double-span traditional timber frame”, *Eng. Struct.*, **98**, 141-150.
- Li, Y.F., Tsai, M.J. and Liao, C.N. (2009), “Effects of tenon depths and bolt constraint conditions on the mechanical behavior of semi-rigid joints of wooden historical buildings”, *Adv. Struct. Eng.*, **12**(3), 349-358.
- Ma, E.N. and Zhao, G.J. (2012), *The monograph on physics for wood*, China Forestry Press, Beijing, China.
- Pang, S.J., Oh, J.K. and Park, J.S. (2011), “Moment-carrying capacity of dovetailed mortise and tenon joints with or without beam shoulder”, *J. Struct. Eng.*, **137**(7), 785-789.
- Parisi, M.A. and Cordie, C. (2010), “Mechanical behavior of double-step timber joints”, *Constr. Build.*

- Mater.*, **24**(8), 1364-1371.
- Sandberg, L.B., Bulleit, W.M. and Reid, E.H. (2000), "Strength and stiffness of oak pegs in traditional timber-frame joints", *J. Struct. Eng.*, **126**(6), 717-723.
- Santana, C.L.O. and Mascia, N.T. (2009), "Wooden framed structures with semi-rigid connections: quantitative approach focused on design needs", *Struct. Eng. Mech.*, **31**(3), 315-331.
- Tannert, T., Lam, F. and Vallee, T. (2010), "Strength prediction for rounded dovetail connections considering size effects", *J. Eng. Mech.*, **136**(3), 358-366.
- Villar, J.R., Guaita, M. and Vidal, P. (2007), "Analysis of the stress state at the cogging joint in timber structures", *Biosystems Eng.*, **96**(1), 79-90.
- Xie, Q.F., Du, B. and Zhang, F.L. (2014), "Theoretical analysis on moment-rotation relationship of dovetail joints for Chinese ancient timber structure buildings", *Eng. Mech.*, **31**(12), 140-146.
- Zhang, X.C., Xue, J.Y. and Zhao, H.T. (2011), "Study on Chinese ancient timber-frame building by shaking table test", *Struct. Eng. Mech.*, **40**(4), 453-469.